Senseable City Lab :.:: Massachusetts Institute of Technology

This paper might be a pre-copy-editing or a post-print author-produced .pdf of an article accepted for publication. For the definitive publisher-authenticated version, please refer directly to publishing house's archive system

COMPUTER-AIDED CIVIL AND INFRASTRUCTURE ENGINEERING

Computer-Aided Civil and Infrastructure Engineering **0** (2017) 1–17

Scalable Structural Modal Identification Using Dynamic Sensor Network Data with STRIDEX

Thomas J. Matarazzo*

Senseable City Laboratory, Massachusetts Institute of Technology, Cambridge, MA 02139, USA

&

Shamim N. Pakzad

Department of Civil and Environmental Engineering, Lehigh University, Bethlehem, PA 18015, USA

Abstract: *This article uses the formulation of the structural identification using expectation maximization (STRIDE) algorithm for compatibility with the truncated physical model (TPM) to enable scalable, output-only modal identification using dynamic sensor network (DSN) data. The DSN data class is an adaptable and efficient technique for storing measurements from a very large number of sensing nodes, which is the case in mobile sensor networks and BIGDATA problems. In this article, the STRIDEX output-only identification algorithm is proposed for the stochastic TPM to estimate structural modal properties (frequencies, damping ratios, and mode shapes) directly from DSN data. The spatial information produced by this novel algorithm, called STRIDEX ("X" for extended), is scalable, as demonstrated in a strategy to construct high-resolution mode shapes from a single DSN data set using a series of independent identification runs. The ability to extract detailed structural system information from DSN data in a computationally scalable framework is a step toward mobile infrastructure informatics in a large urban setting. The performance of the STRIDEX algorithm is demonstrated, using the simulated response of a 5,000 DOF structure, and experimentally, using measurements from two mobile sensor cars, which scanned about 8,000 points on a beam specimen in the laboratory. In the experimental results, a mobile sensor is shown to provide over 120 times more mode shape points than a fixed sensor.*

1 INTRODUCTION

Structural engineers are in perpetual exploration of methodologies that expedite the extraction of information from infrastructure systems. Advancements in sensor technology and innovative data collection techniques target prompt retrieval of structural health metrics, which are essential for short- and long-term structural condition assessments as well as effective maintenance planning. Over the past two decades, structural health monitoring (SHM) applications have incorporated wireless sensing technology (Lynch, 2007), which has facilitated the use of dense sensor arrays in large-scale structures (Ko and Ni, 2005; Lynch et al., 2006; Pakzad et al., 2008). The smart sensing subcategory has offered devices with on-board microprocessors (among other components), which enable enhanced communication, distributed computing, and improved power consumption (Gao et al., 2006; Lynch, 2002; Spencer et al., 2004).

Optimal sensor placement techniques acknowledge high equipment costs and aim to minimize the number of sensors needed to achieve a particular set of structural information from the data, for example, damage detection (Guo et al., 2004; Kim et al., 2000), modal identification (Chang and Pakzad, 2014, 2015; Meo and Zumpano, 2005), and so on. Compressed sensing strategies recognize scalability issues in SHM methods and

*To whom correspondence should be addressed. E-mail: *tomjmat@mit.edu*.

© 2017 *Computer-Aided Civil and Infrastructure Engineering*.
DOI: 10.1111/mice.12298

seek mathematically guided alternatives to brute force when processing very large data sets, that is, BIGDATA (Huang et al., 2014; Matarazzo, et al., 2015b; O'Connor et al., 2014; Yao et al., 2017).

Researchers aspire for data sets that are larger, more informative, and obtained more frequently. Currently in SHM, these data goals are attained by designing and implementing fixed sensor networks (wired or wireless) that are spatially dense (Ko and Ni, 2005; Ni et al., 2009; Pakzad and Fenves, 2009) and/or are incorporated within a long-term monitoring system (Cha et al., 2016; Jang et al., 2010; Kurata et al., 2011, 2013; Soyoz and Feng, 2009; Spiridonakos et al., 2016). Recent implementations of sensing systems with internet connectivity have demonstrated an ability to streamline data collection, storage, and permit real-time results for civil structures, for example, wind-turbines (Smarsly et al., 2012), tall buildings (Kijewski-Correa et al., 2013; Yuen and Mu, 2015), and highway bridges (Zhang et al., 2016). Yet, there remains high value in reducing the cost and labor needed to achieve advanced infrastructure insights (Adeli, 2001; Adeli and Jiang, 2006; Qarib and Adeli, 2015; Sun and Betti, 2015). These constraints are byproducts of the fixed sensor paradigm in SHM: numerous fixed sensors are needed to obtain sufficient spatial information, for example, high-resolution mode shapes, and each with a corresponding cost in dollars and setup/maintenance time. Mobile sensors address the shortcomings of fixed sensors: a single mobile sensor delivers spatial information comparable to that which is retrievable from numerous fixed sensors (Horner et al., 2015; Matarazzo and Pakzad, 2016a; Unnikrishnan and Vetterli, 2012) at a lower cost.

1.1 Toward the acquisition and analysis of crowdsourced infrastructure vibration data

What if the general public had access to portable, high-quality sensors and contributed a volume of informative infrastructure data to SHM every day? Although consumer technology and civil participation have yet to converge in this regard, the recent boom in public smartphone ownership is unprecedented (MediaPost, 2015); the number of connected devices worldwide has already tripled the human population and is multiplying at a faster rate (Hotel News Resource, 2015). This introduction of a mass quantity of different types of sensors including triaxial accelerometers, GPS devices, digital cameras, microphones, and others to the urban environment has quickly impacted how researchers perceive, acquire, and utilize digital data sets (Calabrese et al., 2011; Herrera et al., 2010; Mohan et al., 2008). In the context of SHM, the expected volume of daily mobile smartphone data streams greatly surpasses what a long-term fixed sensor network can supply.

Recent studies have selected smartphones, based on their potential for scalability, to evaluate road quality. For instance, *Pothole Patrol*, a system which gathered and analyzed data from vehicles equipped with a triaxial accelerometer and GPS sensor to assess road surface conditions, was developed by Eriksson et al. (2008) and implemented using seven taxis in Boston, Massachusetts, USA. Potholes were confirmed visually at 39 out of 48 sites identified by the system; the remainders were mostly attributed to sunken manholes, railway crossings, and expansion joints.

SmartRoadSense, a system and mobile application to assess road surface condition from smartphone acceleration records, was proposed by Alessandroni et al. (2014). In experiments, the data were collected by Motorola Moto G smartphones fixed in public bus cabins in Italy; road quality indices were computed for 275 km total. Road surface conditions in India were monitored by Kumar et al. (2016) using data from smartphones mounted on motorbikes, exemplifying a highly technological impact in a country with an emerging economy and a low level of individual smartphone ownership (Pew Research Center, 2016).

The use of stationary smartphones for identifying structural vibration characteristics was discussed by Feng et al. (2015), in which the performances of various common smartphone accelerometers were compared to a reference sensor in laboratory and field dynamic tests. It was concluded that selected smartphone models are capable of recording sinusoidal vibrations with a specified accuracy that depends on the amplitude and frequency of the signal. Power spectral density estimates of vibration test data collected from a bridge in Princeton, New Jersey, USA displayed peaks within 1% of the fundamental frequency, suggesting that smartphone data may be suitable for system identification (SID).

Although smartphone data quality varies, and can suffer from basic signal processing problems, for example, time synchronization errors, noise, clipping, missing data, and so on, the inherent mobility of smartphones poses a more substantial challenge in SHM, because modern models and techniques have been developed exclusively to process data from fixed sensors—not mobile sensors. Furthermore, to fully capitalize on the wealth of public smartphone data that contain infrastructure information, SHM methods must be designed to properly consider data volumes that are magnitudes larger than today's, that is, BIGDATA (this is currently nonstandard in SID and damage detection; Matarazzo et al., 2015a); promising preliminary results indicate that it is no longer prudent to delay these inquires under any

assumption that sufficient computing power might soon be available, for example, Moore's Law.

In particular, the rate at which the SHM community incorporates crowdsourced smartphone data depends on the adaptability and computational scalability of upcoming analytical tools (rather than the evolution of commercial central processing units). These two features target the inherent "variety" and "volume" characteristics of BIGDATA, established by Laney (2001). SHM tools must be (i) adaptable to atypical or heterogeneous sensor networks and (ii) computationally scalable with respect to the number of sensors and sensing nodes represented by the data set. If such a new data stream is truly desired, these two features must be prioritized in the development of data analysis techniques. Otherwise, the data sets applicable to structural vibration analyses will remain those retrieved primarily by researchers, in which case, information will be produced and shared at the current capacity, which provides limited public service. As it will be demonstrated, with its ability to process the dynamic sensor network (DSN) data class (Matarazzo and Pakzad, 2016b), and a strategy to produce high-resolution mode shapes, the proposed extended structural identification using expectation maximization (STRIDEX) method for output-only modal identification is the first to be both adaptable and scalable.

1.2 State of system identification using mobile sensor networks

Over the past decade, there has been notable attention to the problem of identifying modal properties from mobile sensor network data. In summary, these studies have proven that mobile sensor data can contain modal property information. At this time, the SID methods applicable to mobile sensor data cannot produce a full modal property set (frequency, damping, and mode shape) and/or have restrictions on the sensing configuration. One objective in the development of STRIDEX was to provide a comprehensive modal identification, one that includes frequency, damping, and mode shape estimates, using DSN data (a general sensor data class), to match the existing capabilities of SID methods for fixed sensor data.

Frequency identification was explored analytically in Yang et al. (2004), in which equations were developed to describe the dynamic response of a vehicle as it crossed over a bridge. Variations in vehicle speeds and bridge properties were considered and verified using finite element analyses—overall concluding that it is possible to extract the fundamental frequency of the bridge from vehicle vibration (acceleration) data. These findings were verified experimentally by Lin and Yang (2005), in which a tractor-trailer, towing an instrumented cart, drove over the Da-Wu-Lan Bridge in Taiwan. The fundamental frequency of the bridge was successfully extracted from the acceleration spectra of the cart response for three passing speeds (13, 17, and 35 km/h). This was explored further in Yang and Chang (2009) with parametric studies and simulations that considered two bridge frequencies. In Siringoringo and Fujino (2012), an analytical bridge-vehicle model, additional finite element simulations, and further parametric studies on vehicle velocity, vehicle frequency, and bridge frequency were presented; the study concluded with a field experiment at a bridge in southeast Tokyo. The first frequency was successfully identified from the power spectral density (PSD) estimate of the acceleration data collected by an instrumented vehicle, at three speeds (10, 20, and 30 km/h).

With a vehicle-bridge-interaction (VBI) model, a method to estimate bridge damping ratios using acceleration measurements from a moving vehicle was proposed by Gonzalez et al. (2012). The technique assumes Rayleigh structural damping and relies on the double integration of the recorded accelerations to estimate the bridge displacements under the wheel of the vehicle. The method was verified with finite element model simulations that considered various bridge lengths, 21 vehicle speeds, and 9 levels of damping. The sensitivity of these estimates with respect to road surface roughness, measurement noise, and particular modeling inaccuracies were also studied.

A mode shape identification procedure, developed by Marulanda et al. (2016), requires the use of at least two sensors: one mobile sensor and one fixed sensor. The modal frequencies are first identified using the data from the fixed sensor; then, spatially dense mode shapes can be extracted from a space–frequency representation, which is constructed using short-time Fourier transforms. In a theoretical example with a stationary and mobile sensor, assuming noise-free data and known natural frequencies, three mode shapes were accurately identified with 479 points each—further demonstrating the rich spatial information provided by a mobile sensor. In an experimental setup in a laboratory, a sensor car, equipped with a wireless iMote2 sensor, crossed a simply supported beam instrumented with a fixed sensor. The beam was excited by white noise using a dynamic shaker and manually with a rubber hammer. Three mode shapes, with 21 ordinates each, were successfully identified and verified using results from a dense fixed sensor network.

Flexure-based mobile sensing nodes (capable of climbing) were introduced in Zhu et al. (2010) to automate the spatial arrangements of a fixed sensor network, allowing data collection at desirable structural

points with minimal manual labor. In a subsequent study, the team redesigned the units to better navigate structural elements. Four nodes were deployed on a pedestrian steel truss bridge and reported to five sensing configurations, where they paused to collect ambient acceleration data (Zhu et al., 2012). With the use of static reference sensors, three modes were completely and accurately identified from the flexure-based mobile sensing node data, which included detailed mode shapes. The collected data sets had an improved spatial resolution in comparison to a fixed sensor network of the same size, although the potential for spatial information was restricted by the nature of stationary sensing configurations. Accordingly, the data was categorized as fixed sensor data and was processed for SID accordingly with ERA-NExT (James et al., 1993).

Previously, the authors have viewed mobile sensor data as a dense fixed sensor data matrix subjected to the missing data problem. Matarazzo and Pakzad (2016a) presented new equations for the structural identification using expectation maximization (STRIDE) method (Matarazzo and Pakzad, 2016c) to accept data sets with missing observations; the method was successfully applied to simulated mobile sensing data by strategically eliminating entries from a complete data matrix. Although the identified modal properties are accurate and comprehensive, the flaw of this perspective is that of the standard state–space model: the sensing nodes are linked to the model size. As a result, this model lacks scalability because it is computationally inefficient when high-resolution mode shapes are desired.

This article considers a general interpretation of mobile sensor data in which measurements are sampled as sensors move in space. With this definition, a mobile sensor network reduces to a fixed sensor network if the positions of the sensors do not change over time. The following sections review how mobile sensor data are classified as DSN data and can be modeled exactly using the truncated physical model (TPM).

In past work by the authors in this framework, an experimental mobile sensing testbed was developed and a preliminary version of STRIDEX was successfully applied (Horner et al., 2015; Matarazzo et al., 2016a). In one study, three vertical modes were identified using four mobile sensors; mode shapes contained up to 150 points—although fixed sensor results were unavailable for comparison (Matarazzo et al., 2016b; Matarazzo et al., 2016a).

1.3 Contributions

This article builds on fundamental knowledge and practice of DSNs, a data class that includes mobile sensor networks and BIGDATA. The TPM (Matarazzo and Pakzad, 2016b) was introduced as an efficient approach to include DSN data into the model of the structural system. An extension of the STRIDE output-only identification algorithm (Matarazzo and Pakzad, 2016c) is presented, and named STRIDEX ("X" for extended), for the TPM. The proposed technique has four novel features:

(1) Comprehensive and convenient: estimates frequencies, damping, and mode shapes simultaneously.
(2) Adaptable: there are no methodological restrictions on sensor arrangement or mobility as long as the positions of each sensor are known for all samples.
(3) Scalable information: with a new virtual probing location (VPL) assignment, an additional identification run can produce a new set of mode shape ordinates from the same set of DSN data.
(4) Computationally scalable: (i) the size of the TPM is independent of the density of the spatial grid applied during measurement and (ii) in the construction of high-resolution mode shapes, the computational needs of individual runs are nearly equivalent to one another.

The first two features match the capabilities of traditional SID methods in regards to fixed sensor data. The third feature harnesses DSNs' high capacity for spatial information, which enables high-resolution mode shape estimates using few sensors. Finally, the computational scalability of STRIDEX (along with its adaptability) is conducive for processing large data streams and BIGDATA volumes.

There are two central technical challenges within STRIDEX, which result from the inherent presence of spatial discontinuities in DSN data matrices: (i) the time variant nature of the observation equation and (ii) the apparent reliance of the TPM on mode shape information prior to identification. These complications are addressed in Section 3.3.

An output-only modal identification method that can successfully process DSN data is applicable to crowdsourced smartphone data. Furthermore, high-resolution mode shapes are highly valuable to SHM processes that are sensitive to spatial features such as damage detection based on mode shape curvature (Abedl Wahab and De Roeck, 1999; Chandrashekhar and Ganguli, 2009; Pandey et al., 1991). It is worthwhile to note that, more generally, the objective of this article is to extract some form of structural information from the DSN data class using a time-series model (in the state-space formulation). Because such models (and variations, e.g., ARMA; Box et al., 2008) and their parameters (or

coefficients) play a fundamental role in numerous damage detection and model updating algorithms (Carden and Brownjohn, 2008; Nigro et al., 2014; Shahidi et al., 2015; Yao and Pakzad, 2012), it is suggested that portions of this work may also serve as a framework for processing DSN data in SHM in a more generic application.

2 MODELING DYNAMIC SENSOR NETWORK MEASUREMENTS FROM A STRUCTURAL SYSTEM

2.1 Review of dynamic sensor networks

DSN data (Matarazzo and Pakzad, 2016b) are a general data class in which the sensor configuration changes during measurement. DSN data are scalable with respect to sensor quantity; through concatenation, additional measurement channels may be included in the data matrix without affecting its dimensions. DSNs have a high capacity for spatial information and store structural responses in a compact data matrix. By contrast, fixed sensor network data contain costly, yet restricted spatial information. For instance, in SID, a dense fixed sensor network can have substantial equipment and processing requirements: a sensing device must be installed at every point where a mode shape ordinate is desired, whereas the addition of a measurement channel to the data set affects computational costs cubically (Matarazzo et al., 2015b)—a result comparable to that of increasing model orders for stabilization diagrams (Chang and Pakzad, 2013a, b).

DSNs account for changes in sensing configurations with spatial discontinuities in the data matrix. In the applications presented, the switching times are known and intentional; it is the source of these spatial discontinuities which characterize the DSN type as either online, offline, or hybrid (a detailed explanation of these types is available in Matarazzo and Pakzad (2016b)). At each time step, k, the sensors' locations are $\boldsymbol{s}_k^O \in \mathbb{R}^{N_O}$, where the superscript ^{O} indicates the set of observed sensing nodes, which covers N_O points at every time step and N sensing nodes over the entire time series.

2.2 Stochastic truncated physical model

In this section, the stochastic TPM is presented to consider randomly driven states and noisy observations in the output-only identification problem (ambient vibration data). For best comprehension, it is recommended that the reader reviews the deterministic TPM, as introduced in Matarazzo and Pakzad (2016b) prior to delving into the following equations. Note, in this article, there exist some slight symbolic differences in regards to mathematical entities; a notation table with descriptions follows the References.

In the standard state-space model, the sensing nodes are coupled with the state variable (model DOF); thus a dense grid applied during measurement requires a highly complex dynamic model (Matarazzo and Pakzad, 2016b). In the TPM, the system states do not rely on the sensing nodes covered in the DSN data. As a result, an intuitive relationship is formed between DSN observations and model size.

In the TPM, the state variable represents the truncated physical structural response at user-selected VPLs, which are N_α static points, defined as $\boldsymbol{s}^\alpha \in \mathbb{R}^{N_\alpha}$. The VPLs are the points at which the structural responses will be modeled, as well as where mode shape ordinates will be evaluated. The VPL choice is a modeling decision and therefore independent of the DSN data. The asterisk superscripts in TPM entities presented in Matarazzo and Pakzad (2016b) are omitted here for simplicity. More specifically, the TPM state vector, $\boldsymbol{x}_k \in \mathbb{R}^{pN_\alpha}$, and state matrix, $A \in \mathbb{R}^{pN_\alpha \times pN_\alpha}$, are $\boldsymbol{x}_k^*$ and A^* from equations (31) and (28), respectively, in Matarazzo and Pakzad (2016a), where p is the model order. The observation matrix, $C \in \mathbb{R}^{M \times pN_\alpha}$, is defined as $C \equiv \Phi^\alpha C^*$ (C^* is found within equations (30) and (33) of Matarazzo and Pakzad (2016a)) to reduce the total number of unknown parameters; the identification of this product is sufficient for evaluating pN_α structural mode shapes at the VPLs. The observations $\boldsymbol{y}_k \in \mathbb{R}^{N_O}$ are the measurements of the DSN data at time-step k. Finally, the *mode shape regression* (MSR) term, $\Omega_k \in \mathbb{R}^{N_O \times M}$, is defined as $\Omega_k \equiv \Phi_k^O(\Phi^\alpha)^{-1}$ and relates the modal ordinates of the VPL (denoted by superscript $^\alpha$) to the sensor locations (observations) at time-step k (denoted by superscript ^{O}). This time-variant term is synchronized with the spatial discontinuities in the DSN data because it is a function of the sensors' locations. For the purpose of establishing the identification framework, it is first assumed that the MSR term is known at all time steps. This assumption is revisited in Section 3.3.

Equations (1) and (2) are the state and observation equations for the stochastic TPM for time-steps $k = 1,\ 2,\ \cdots,\ K$ and Equations (3)–(5) define aleatory variables.

$$\boldsymbol{x}_k = A\boldsymbol{x}_{k-1} + \boldsymbol{\eta}_k \tag{1}$$

$$\boldsymbol{y}_k = \Omega_k\, C\boldsymbol{x}_k + \boldsymbol{v}_k \tag{2}$$

$$\boldsymbol{x}_1 \sim N\left(\bar{\boldsymbol{\mu}}, \bar{V}\right) \tag{3}$$

$$\boldsymbol{\eta}_k \sim N\left(\boldsymbol{0}, Q\right) \tag{4}$$

$$\boldsymbol{v}_k \sim N\left(\boldsymbol{0}, R\right) \tag{5}$$

As in the original STRIDE formulation, the state input $\boldsymbol{\eta}_k \in \mathbb{R}^{pN_\alpha}$ and observation error/noise $\boldsymbol{v}_k \in \mathbb{R}^{N_O}$ terms are assumed to be zero-mean and uncorrelated Gaussian vectors with diagonal covariance matrices $Q \in \mathbb{R}^{pN_\alpha \times pN_\alpha}$ and $R \in \mathbb{R}^{N_O \times N_O}$, respectively. The superparameter, Ψ, which is updated with each iteration, is defined in Equation (6); note the absence of the time-variant parameter Ω_k.

$$\Psi = \left(\bar{\boldsymbol{\mu}}, \bar{V}, A, Q, C, R\right) \tag{6}$$

The complete data log-likelihood function of the TPM is a mixture of three Gaussian densities that depend on the superparameter:

$$\begin{aligned}\ln\left(L_{X,Y}\left(\Psi\right)\right) = & -\frac{\left(N_O + pN_\alpha\right)K}{2}\ln\left(2\pi\right) \\ & -\frac{1}{2}\ln\left|\bar{V}\right| - \frac{1}{2}\left(\boldsymbol{x}_1 - \bar{\boldsymbol{\mu}}\right)^T \bar{V}^{-1}\left(\boldsymbol{x}_1 - \bar{\boldsymbol{\mu}}\right) \\ & -\frac{1}{2}\ln\left|R\right| - \frac{1}{2}\sum_{k=1}^{K}\left(\boldsymbol{y}_k - \Omega_k C\boldsymbol{x}_k\right)^T R^{-1}\left(\boldsymbol{y}_k - \Omega_k C\boldsymbol{x}_k\right) \\ & -\frac{1}{2}\ln\left|Q\right| - \frac{1}{2}\sum_{k=2}^{K}\left(\boldsymbol{x}_k - A\boldsymbol{x}_{k-1}\right)^T Q^{-1}\left(\boldsymbol{x}_k - A\boldsymbol{x}_{k-1}\right)\end{aligned} \tag{7}$$

Because the complete data (states) are unmeasured, the conditional expectations of the states are computed based on the observations and a superparameter estimate. The conditional expectation of the log-likelihood function under the observations $Y = \boldsymbol{y}_1, \ldots, \boldsymbol{y}_K$ and the superparameter at iteration j is defined in Equation (8).

$$G\left(\Psi_{j+1}|\Psi_j\right) = E\left[\ln\left(L_{X,Y}\left(\Psi_j\right)\right)|Y\right] \tag{8}$$

With the stochastic TPM and its parameters specified, the next section discusses the equations needed to identify the maximum likelihood estimate (MLE) of the superparameter.

3 STRIDEX ALGORITHM

The procedure and the goal of STRIDEX remains the same as those of STRIDE (Matarazzo and Pakzad, 2016c). The algorithm begins with an initial parameter set $\Psi_0 = (\bar{\boldsymbol{\mu}}_0, \bar{V}_0, A_0, Q_0, C_0, R_0)$ and iterates between the expectation and maximization steps (E-step and M-step, respectively), maximizing the conditional log-likelihood function $G(\Psi_{j+1}|\Psi_j)$ (henceforth G) each time. The procedure continues until the slope of G is nearly zero, that is, below a nominal slope threshold (it is suggested to start with $\theta = 5 \times 10^{-4}$). Some modifications are needed in the original E-step equations to adjust to the time-variant nature of the observation equation in the TPM (Equation (2)). For the M-step, the update formulae must be derived analytically from the log-likelihood function in Equation (8). Otherwise, the procedures for initial superparameter estimation and guidelines for model order selection may be implemented as specified for STRIDE in Matarazzo and Pakzad (2016c).

3.1 E-step for STRIDEX

The goal of the E-step is to provide minimum mean-squared error (MSE) estimates and covariances for the hidden state variable. Given the data and a superparameter estimate, the conditional expectation of the states and their covariances are defined in Equations (9)–(11).

$$\hat{\boldsymbol{x}}_{k|K} = E\left[\boldsymbol{x}_k|Y\right] \tag{9}$$

$$\hat{V}_{k,k|K} = E\left[\left(\boldsymbol{x}_k - \hat{\boldsymbol{x}}_{k|K}\right)^T\left(\boldsymbol{x}_k - \hat{\boldsymbol{x}}_{k|K}\right)|Y\right] \tag{10}$$

$$\hat{V}_{k,k-1|K} = E\left[\left(\boldsymbol{x}_k - \hat{\boldsymbol{x}}_{k|K}\right)^T\left(\boldsymbol{x}_{k-1} - \hat{\boldsymbol{x}}_{k-1|K}\right)|Y\right] \tag{11}$$

These estimates are achieved using the recursive Kalman filter and Rauch-Tung-Striebel (RTS) equations presented along STRIDE (Matarazzo and Pakzad, 2016c) with the following change of variables: given the time-varying observation equation, it is convenient to implement an equivalent observation matrix at each time step, k, equal to $C_k^{(eq)} = \Omega_k C$, where Ω_k and C are those within Equation (2). With this substitution, the filtered and smoothed estimates for the states and state covariances may be computed for a given superparameter.

3.2 M-step for STRIDEX

The updating formulae for the unknown parameters are obtained through the maximization of the conditional log-likelihood function at iteration j, that is, the solution of $\partial G/\partial\psi = 0$ for $\psi \in \Psi$. Despite the new likelihood function for the stochastic TPM in Equation (7), the updating equations for A_{j+1}, Q_{j+1}, $\bar{\boldsymbol{\mu}}_{j+1}$, and $\bar{V}_{j+1}$ end up identical to those in STRIDE because they are uninvolved in the observation equation.

$$\begin{aligned}A_{j+1} = & \sum_{k=1}^{K}\left[\hat{\boldsymbol{x}}_{k|K}\hat{\boldsymbol{x}}_{k-1|K}^T + \hat{V}_{k,k-1|K}\right] \\ & \times\left(\sum_{k=1}^{K}\left[\hat{\boldsymbol{x}}_{k-1|K}\hat{\boldsymbol{x}}_{k-1|K}^T + \hat{V}_{k-1,k-1|K}\right]\right)^{-1}\end{aligned} \tag{12}$$

$$Q_{j+1} = \frac{1}{K-1}\left(\sum_{k=2}^{K}\left(\hat{\boldsymbol{x}}_{k|K}\hat{\boldsymbol{x}}_{k|K}^{T} + \hat{V}_{k,k|K}\right) - A_{j+1}\sum_{k=2}^{K}\left(\hat{\boldsymbol{x}}_{k-1|K}\hat{\boldsymbol{x}}_{k|K}^{T} + \hat{V}_{k-1,k|K}\right)\right) \quad (13)$$

$$\bar{\boldsymbol{\mu}}_{j+1} = \hat{\boldsymbol{x}}_{1|K} \quad (14)$$

$$\bar{V}_{j+1} = \hat{V}_{1,1|K} \quad (15)$$

Next, the two updating formulae pertaining to observation equation parameters are derived. A shorthand notation $E^{(Y,j)}[()] = E[()|Y, \Psi_j]$ is adapted to simplify a recurring conditional expectation. Equation (16) is the partial derivative of G with respect to the observation matrix C.

$$\frac{\partial G}{\partial C} = 0 = \frac{\partial}{\partial C}\left(E^{(Y,j)}\left[-\frac{1}{2}\sum_{k=1}^{K}(\boldsymbol{y}_k - \Omega_k C\boldsymbol{x}_k)^T R^{-1} \times (\boldsymbol{y}_k - \Omega_k C\boldsymbol{x}_k)\right]\right) = \sum_{k=1}^{K}\left(\Omega_k^T \boldsymbol{y}_k E^{(Y,j)}\left[\boldsymbol{x}_k^T\right] - \Omega_k^T\Omega_k C E^{(Y,j)}\left[\boldsymbol{x}_k\boldsymbol{x}_k^T\right]\right) \quad (16)$$

$$0 = vec\left(\sum_{k=1}^{K}\Omega_k^T \boldsymbol{y}_k E^{(Y,j)}\left[\boldsymbol{x}_k^T\right]\right) - vec\left(\sum_{k=1}^{K}\Omega_k^T\Omega_k C E^{(Y,j)}\left[\boldsymbol{x}_k\boldsymbol{x}_k^T\right]\right)$$

$$0 = vec\left(\sum_{k=1}^{K}\Omega_k^T \boldsymbol{y}_k E^{(Y,j)}\left[\boldsymbol{x}_k^T\right]\right) - \left(\sum_{k=1}^{K}E^{(Y,j)}\left[\boldsymbol{x}_k\boldsymbol{x}_k^T\right]\otimes\Omega_k^T\Omega_k\right) vec\,(C)$$

$$vec\ (C_{j+1}) = \left(\sum_{k=1}^{K}E^{(Y,j)}\left[\boldsymbol{x}_k\boldsymbol{x}_k^T\right]\otimes\Omega_k^T\Omega_k\right)^{-1} \times vec\left(\sum_{k=1}^{K}\Omega_k^T \boldsymbol{y}_k E^{(Y,j)}\left[\boldsymbol{x}_k^T\right]\right) \quad (17)$$

In Equation (17), the individual terms of Equation (16) are vectorized and the Kronecker product is implemented to remove the observation matrix from the summation of the second-term. The last two lines of Equation (17) show the new M-step formula for the observation matrix C_{j+1}.

Next, the updating formula for the observation noise covariance is considered; Equation (18) shows the partial derivative of G with respect to R^{-1}. The newest observation matrix, C_{j+1}, is used in the observation noise covariance updating formula in Equation (19).

$$\frac{\partial G}{\partial R^{-1}} = 0 = \frac{\partial}{\partial R^{-1}}\left(E^{(Y,j)}\left[-\frac{K}{2}ln\,(R) - \frac{1}{2}\sum_{k=1}^{K}(\boldsymbol{y}_k - \Omega_k C\boldsymbol{x}_k)^T R^{-1}(\boldsymbol{y}_k - \Omega_k C\boldsymbol{x}_k)\right]\right)$$

$$= \frac{K}{2}R - \frac{1}{2}\sum_{k=1}^{K}\left(\boldsymbol{y}_k\boldsymbol{y}_k^T - \boldsymbol{y}_k E^{(Y,j)}\left[\boldsymbol{x}_k^T\right]C^T\Omega_k^T - \Omega_k C E^{(Y,j)}\left[\boldsymbol{x}_k\right]\boldsymbol{y}_k^T + \Omega_k C E^{(Y,j)}\left[\boldsymbol{x}_k\boldsymbol{x}_k^T\right]C^T\Omega_k^T\right)$$

$$R_{j+1} = \frac{1}{K}\sum_{k=1}^{K}\left(\boldsymbol{y}_k\boldsymbol{y}_k^T - \boldsymbol{y}_k E^{(Y,j)}\left[\boldsymbol{x}_k^T\right]C^T\Omega_k^T - \Omega_k C E^{(Y,j)}\left[\boldsymbol{x}_k\right]\boldsymbol{y}_k^T + \Omega_k C E^{(Y,j)}\left[\boldsymbol{x}_k\boldsymbol{x}_k^T\right]C^T\Omega_k^T\right) \quad (18)$$

$$R_{j+1} = \frac{1}{K}\sum_{k=1}^{K}\left(\boldsymbol{y}_k\boldsymbol{y}_k^T - \boldsymbol{y}_k E^{(Y,j)}\left[\boldsymbol{x}_k^T\right]C_{j+1}^T\Omega_k^T - \Omega_k C_{j+1}E^{(Y,j)}\left[\boldsymbol{x}_k\right]\boldsymbol{y}_k^T + \Omega_k C_{j+1}E^{(Y,j)}\left[\boldsymbol{x}_k\boldsymbol{x}_k^T\right]C_{j+1}^T\Omega_k^T\right) \quad (19)$$

With the M-step formulae provided in this section, the superparameter for the TPM can be updated and the algorithm proceeds to the next iteration, namely $j+1$ (Equation (20)).

$$\Psi_{j+1} = \left(\bar{\boldsymbol{\mu}}_{j+1}, \bar{V}_{j+1},\ A_{j+1}, Q_{j+1}, C_{j+1},\ R_{j+1}\right) \quad (20)$$

The procedure continues until the likelihood slope is below the threshold, θ. The estimated modal properties are computed from the MLE of the superparameter namely $\Psi_{ML} = (\bar{\boldsymbol{\mu}}_{ML}, \bar{V}_{ML},\ A_{ML}, Q_{ML}, C_{ML},\ R_{ML})$. The modal properties corresponding to the MLE are computing using the state matrix, A_{ML}, and observation matrix, C_{ML}. An eigendecomposition of A_{ML} produces the diagonal eigenvalue matrix, Λ_{ML}, and the eigenvector matrix, Γ_{ML}. The estimated natural frequency and damping ratio vectors in Equations (21) and (22), respectively, are computed using the diagonal elements of Λ_{ML}. In Equation (23), the estimated mode shape

ordinates correspond to the coordinates of the VPLs.

$$\hat{f} = \frac{2\pi \left| ln\left[diag\left(\Lambda_{ML} \right) \right] \right|}{\Delta t} \tag{21}$$

$$\hat{\xi} = -\cos\left(\measuredangle ln\left[diag\left(\Lambda_{ML} \right) \right] \right) \tag{22}$$

$$\hat{\Phi} = C_{ML} \Gamma_{ML} \tag{23}$$

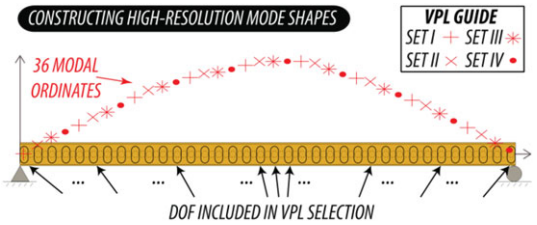

Fig. 1. Illustration depicting the construction of a mode shape with 36 ordinates from four unique sets of nine VPLs.

3.3 On the estimation of the mode shape regression term

With a time-variant observation equation in the TPM, the linear time-invariant (LTI) dynamic system depends on a time-varying parameter, namely the mode shape regression (MSR) term, Ω_k. Thus it is appropriate to categorize the identification of the TPM as a linear parameter-varying (LPV) model identification problem (Bamieh and Giarré, 2002; Lee and Poolla, 1999; Tóth et al., 2009; Verdult and Verhaegen, 2002). In this framework, the observations, Y, are dependent on the LTI system and a scheduling signal (Toth, 2010). In particular, the so-called schedule of the observations is the sensor-position matrix of the DSN data ($\boldsymbol{s}_k^O$ at time step, k).

In the preceding sections, it was assumed the exact MSR relations, Ω_k, were available with the data; however, in practice, this is not the case because the mode shapes are unavailable prior to system identification thus, these relations must be estimated. With the TPM, the unknown MSR matrix may be accurately approximated using *sinc* or *spline* basis functions (Matarazzo and Pakzad, 2016b). Through this relation, all unknown model parameters are time invariant and the identification of the TPM is considerably simplified.

Influenced by Moheimani et al. (2003), Matarazzo and Pakzad (2016b) reformulated Whitaker-Kotelnikov-Shannon (WKS) (Kotelnikov, 1933; Shannon, 1998; Whittaker, 1915, 1929) sampling reconstruction theory exclusively for spatial interpolation of structural mode shapes. More specifically, mode shape ordinates at one set of sensing nodes were related to mode shape ordinates at another set through basis functions. The relation demonstrated that a *sinc* basis can be used as an estimator of the MSR term, say $\hat{\Omega}_k$, in the TPM. It was shown that a *B-spline* basis could also reasonably estimate the MSR term, with less accuracy. To implement this approach for DSN data in the TPM, the locations of all sensors in the DSN must be known for each sample and VPLs must be selected. For optimal reconstruction and simplicity, it was recommended that the VPLs be spaced uniformly (Matarazzo and Pakzad, 2016b). As a review, the VPLs are a modeling choice, achieved by defining the MSR estimator:

$$\hat{\Omega}_k = \begin{bmatrix} sinc\left(\frac{1}{\Delta s^\alpha} \left(\boldsymbol{s}_k^O - s_1^\alpha \right) \right) \\ sinc\left(\frac{1}{\Delta s^\alpha} \left(\boldsymbol{s}_k^O - s_2^\alpha \right) \right) \\ \vdots \\ sinc\left(\frac{1}{\Delta s^\alpha} \left(\boldsymbol{s}_k^O - s_{N_\alpha}^\alpha \right) \right) \end{bmatrix}^T \tag{24}$$

where $\boldsymbol{s}_k^O$ is the vector of the positions of the observations in the DSN data set at sample k, s_i^α is the location of the ith VPL (N_α total), and Δs^α is the distance between the VPLs. The spacing of the VPLs must be chosen to avoid spatial aliasing. The condition for perfect reconstruction of the Mth mode of a uniform simply supported beam with length L, is $\Delta s^\alpha < L/M$ (Matarazzo and Pakzad, 2016b; Moheimani et al., 2003). Although, this rule is not unique to VPLs; it governs the arrangement of a fixed sensor network.

3.4 Scalable strategy for high-resolution mode shapes

This subsection discusses the strategy to construct high-resolution mode shapes by compiling STRIDEX results. The rich spatial information available in DSN permits the estimation of mode shapes at a theoretically unlimited number of points, because they do not necessarily need to coincide with sensing nodes. After a STRIDEX implementation, the estimated mode shape matrix contains one set of modal ordinates for each identified mode, which corresponds to the chosen VPLs. The identification process can be repeated using the same DSN data set, yet with new (ideally non-overlapping) VPLs, to increase the total quantity of modal ordinates available. This process may be repeated as deemed necessary by the analyst. Once the desired number of modal ordinates has been reached, they are aggregated into a high-resolution mode shape.

Figure 1 illustrates this strategy in which 9 mobile sensors provide a mode shape with 36 ordinates. Consider a DSN data set, Y, with size $K \times N_O$, where $N_O = 9$. Nine uniformly spaced VPLs are chosen ($N_\alpha = N_O = 9$),

and STRIDEX processes the DSN data, producing 9 modal ordinates at "Set I"; these results are stored. Next, a new set of VPLs is chosen while analyzing the same DSN data with STRIDEX; as a result, 9 modal ordinates are added (18 total). This procedure continues twice more to produce 18 additional unique modal ordinates for each identified mode shape. Note these analyses are independent of one another. Finally, the modal ordinates (four sets of nine) are aggregated so that each identified mode shape contains 36 points. Note a similar result can be obtained using data from four mobile sensors and applying nine different sets of four VPLs.

This strategy is scalable both in regards to spatial information and computational requirements. Similar to STRIDE, STRIDEX is most computationally sensitive to the model order, p, the number of observations in the DSN, N_O, and the slope threshold, θ (a detailed account of the computational operations within STRIDE is available in Matarazzo and Pakzad (2016c)); the new E- and M-step equations specific to STRIDEX have a negligible impact on the overall computational costs. Through the application of this strategy, only the VPLs are updated, all other settings remain unchanged, that is, data size, model order, slope threshold, and so on. Thus, the computational needs of individual STRIDEX runs are practically equivalent to one another. The number of iterations required to achieve the prescribed slope threshold will vary marginally with each run. It should be emphasized that each additional STRIDEX run can extract further mode shape ordinates from the same DSN data set; this scalable information feature is exemplified in the following application sections.

4 NUMERICAL VALIDATION OF STRIDEX WITH 5,000-DOF BEAM

In this section, a uniform 5,000-DOF beam, with natural frequencies ranging from 0.27 to 98 Hz and 1% damping in all modes, is analyzed. The structure is subjected to a vertical white noise ground motion at the supports with a frequency cut off at 25 Hz. The objective is to identify the first four modal properties of this system using DSN data.

4.1 Description of mobile sensor network data

In this simulation, each sensing node was modeled as a lumped mass DOF in the beam. Figure 2 illustrates how the simulated network of six mobile sensors scanned 4,992 sensing nodes in unison, with two back-and-forth motions, passing each node at least four times. For wide coverage, mobile sensors were equally spaced at 715 nodes apart and were each designated a zone with

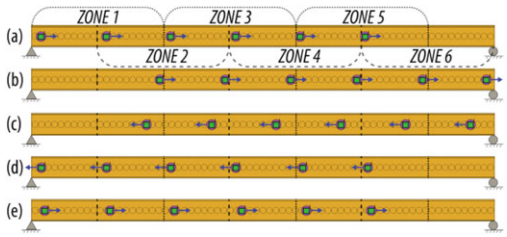

Fig. 2. A network of six equally-spaced mobile sensors scans 4,992 points on the beam at the same speed. Each sensor scans its designated zone four times, twice in each direction, without pause: (a) sensors begin forward scan; (b) sensors complete forward scan; (c) sensors begin reverse scan; (d) sensors complete reverse scan; (e) sensors begin next scanning cycle and eventually stop at their starting positions (step not shown).

a width of 1,430 nodes (50% overlap). The nodes in overlapping portions of these zones were each measured eight times, that is, double coverage for sensing nodes within the central 71%. The corresponding DSN data were calculated as the observations of the time-variant TPM, using the exact MSR relations. Alternatively, this data could have been generated by either the standard or modal TPM discussed in Matarazzo and Pakzad (2016b). For the minimum model size, the number of modes included in the response was set equal to the observation size in the DSN data matrix ($M = N_O$). In the case of online DSN data, the observation size is also equal to the number of sensor channels, that is, $N_O = N_{mc}$. In this example, $M = N_O = N_{mc} = 6$.

The mobile sensors recorded acceleration at 50 Hz, moving to the next sensing node (DOF for discretized systems) in their respective routes after each sample. The DSN data was composed of six observations with 3,328 samples each, which represented the vibrations of 4,992 points over the course of about 67 seconds. Finally, 1% random noise was added to the DSN data to simulate measurement errors.

4.2 Selection of VPLs and modal identification results

With the DSN data specified, the analyst can choose the VPLs. To preserve the minimum model size of the TPM, the number of VPLs, N_α, should be set equal to the number of modes included in the response, M; that is, $N_\alpha = M = 6$. In this example, 24 ordinates are targeted for each mode shape; therefore, it is necessary to select four sets of six VPLs.

Table 1 details the four VPL sets considered; these are the points at which mode shapes will be evaluated in SID. In all sets, the VPLs are spaced equally to the nearest integer (either by 714 or 715 nodes). For

Table 1
Each VPL set includes six points (DOFs in this example) and dictates where on the structure the mode shapes will be evaluated during identification. Four VPL sets are detailed below: $\boldsymbol{s}^{\alpha(I)}$, $\boldsymbol{s}^{\alpha(II)}$, $\boldsymbol{s}^{\alpha(III)}$, and $\boldsymbol{s}^{\alpha(IV)}$. In each set, the VPLs are spaced equally (by 714 or 715) to the nearest integer

VPL Set	s_1^α	s_2^α	s_3^α	s_4^α	s_5^α	s_6^α
$\boldsymbol{s}^{\alpha(I)}$	571	1,285	2,000	2,714	3,428	4,142
$\boldsymbol{s}^{\alpha(II)}$	714	1,428	2,142	2,857	3,571	4,285
$\boldsymbol{s}^{\alpha(III)}$	857	1,571	2,285	2,999	3,714	4,428
$\boldsymbol{s}^{\alpha(IV)}$	1,000	1,714	2,428	3,142	3,857	4,571

clarification, the DSN data is independent of the VPL selection; although it is true that in this case, the mobile sensors share this spacing, it is coincidental and was only chosen for illustration. Furthermore, the VPL sets are essentially shifted versions of one another. For instance, the points in $\boldsymbol{s}^{\alpha(I)}$ are 143 (142 for s_3^α) nodes apart from those in $\boldsymbol{s}^{\alpha(II)}$.

The STRIDEX method was performed four times, once for each VPL set, using the same DSN data. A model order of four, $p = 4$, and a slope threshold of $\theta = 5 \times 10^{-4}$ (the standard value) were selected and the initial estimates for A_0 and C_0 were provided by ERA-OKID-OO (Chang and Pakzad, 2013b) (also $p = 4$). The remaining parameters were set in accordance with the initialization guidelines for STRIDE (Matarazzo and Pakzad, 2016c): $\bar{\boldsymbol{\mu}}_0$ was the zero vector with size pN_α, whereas $\bar{V}_0$, Q_0, and R_0 were the identity matrices with sizes pN_α, pN_α, and N_O, respectively.

Each STRIDEX run produced a comprehensive set of modal property estimates. In Table 2, the frequency and damping estimates computed for each VPL set are compared with the exact MDOF values; the STRIDEX mean and the coefficient of variation (CoV) values were computed based on the VPL results and provide a measure of precision. The individual and mean STRIDEX frequency estimates matched the exact values for each mode. The STRIDEX CoV for the frequencies was also low, showing a consistent accuracy. The STRIDEX damping ratio estimates were also quite close to the true values; this is significant because damping estimates in output-only SID are typically associated with large error margins (Au, 2013; Chang and Pakzad, 2013b). In particular, the mean damping estimates for modes two and four were within 8% and 3% of the exact values, respectively. The CoV of the STRIDEX damping estimates also indicate consistency. Overall, the accuracies of the frequency and damping estimates provided by STRIDEX are aligned with those achieved in fixed sensor SID.

Figure 3 superposes the high-resolution mode shapes, estimated using the mobile sensor data, on the exact values at all 24 DOFs under consideration. To reiterate, modal ordinates at twenty-four unique beam locations were estimated using only six sensors. In other words, each mobile sensor provided the spatial information of four fixed sensors. Moreover, as it will be demonstrated more explicitly in the following experimental application, STRIDEX shows that mobile sensors can provide practically unlimited spatial information in the scanned region.

In addition to the high quantity of modal ordinates provided using only six mobile sensors, the accuracy of the estimates is also noteworthy. The consistency between the STRIDEX mode shapes and the exact values were evaluated using the modal assurance criterion (MAC) and are displayed in Figure 3. All four values were greater than 0.98, of which three surpassed 0.99. Within the third mode, there is one point (at DOF 3,428) that is misaligned; the magnitude of this modal ordinate is correct, although the reversed sign reduces the MAC value for the shape.

In summary, the STRIDEX method demonstrated its ability to produce reliable modal property estimates for frequencies, damping ratios, and dense mode shapes for a 5,000-DOF beam. The estimation efficiency of the mode shapes is particularly promising: the accuracy and scalability of STRIDEX are displayed.

5 EXPERIMENTAL APPLICATION

This section presents an experimental implementation of a mobile sensor network, which scans the vibrations of a flexible steel beam specimen, a platform introduced in Horner et al. (2015). The resulting DSN data is processed with the STRIDEX algorithm to determine comprehensively the fundamental mode. For validation, fixed sensor data was also collected and processed for SID using ERA-NExT and STRIDE.

5.1 Mobile sensing platform and beam specimen

The beam specimen (pictured in Figure 4a) is a simply supported steel plate with an adjustable posttensioning system, which can control the midspan deflection while permitting analyses of various dynamic systems. The beam is a 6.35-mm (¼ in) thin steel plate that is 635 mm (25 in) wide by 3.66 m (12 ft) long, and is supported 305 mm (12 in) from each end. Beneath the plate, a steel shore post (manufactured by Ellis—not visible in Figure 4a), with its adjustable length, provides a selectable horizontal posttensioning force on the supports.

Table 2
STRIDEX frequency and damping estimates for the first four modes of the 5,000-DOF beam and exact values

	Frequencies (Hz)				*Damping ratios (%)*			
VPL set	f_1	f_2	f_3	f_4	ζ_1	ζ_2	ζ_3	ζ_4
$\boldsymbol{s}^{\alpha(I)}$	0.2682	1.094	2.438	4.341	4.497	1.126	0.839	1.114
$\boldsymbol{s}^{\alpha(II)}$	0.2685	1.093	2.440	4.342	2.077	1.038	0.858	0.966
$\boldsymbol{s}^{\alpha(III)}$	0.2684	1.092	2.437	4.338	3.558	1.249	0.916	0.970
$\boldsymbol{s}^{\alpha(IV)}$	0.2694	1.095	2.439	4.348	1.494	0.905	0.922	1.059
Mean	0.2686	1.093	2.439	4.342	2.906	1.079	0.884	1.027
CoV ($\times 10^{-4}$)	18.97	10.56	5.940	9.507	4716	1344	469.4	703.7
Exact value	0.2735	1.088	2.448	4.352	1.000	1.000	1.000	1.000

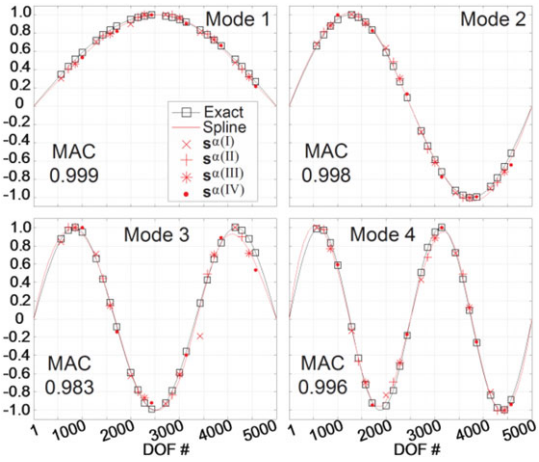

Fig. 3. High-resolution mode shape estimates for the first four modes. Each shape contains 24 modal ordinates, which are compared with the exact values.

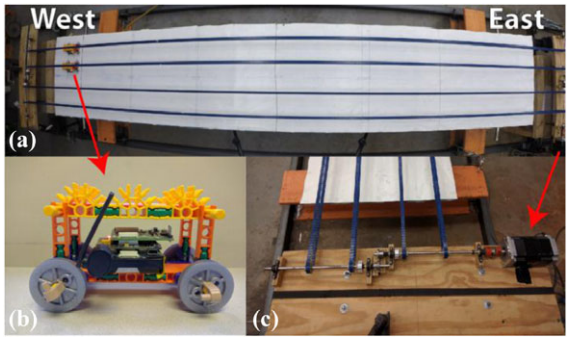

Fig. 4. (a) Aerial photo of beam specimen at Lehigh University. Two mobile sensor cars are shown at their starting positions; (b) mobile sensor car equipped with a wireless accelerometer; (c) step motor, shaft assemblage, and four belts.

At both ends of the specimen, there are wooden pedestals that carry the motor-driven pulley system. Rotational shafts with gears were mounted on the pedestals and the step motor (STAC6-Si by Applied Motion) was installed on the East one. Figure 4a shows four blue belts, which extend over the specimen, from one pedestal to the other, and make contact with the roof of the mobile sensor cars parked at the West support. Figure 4b shows a close-up of a sensor car, which was used in Horner et al. (2015) and was constructed out of small plastic components. Figure 4c shows the step-motor assemblage on the East pedestal that drives the pulley system. Each car carries an IPR2420 Imote2 configured with TinyOS bootloader (Pakzad et al., 2008), an IBB2400CA battery board (three 1.2 V batteries), and an ISM400 sensor board (Spencer, 2011).

A script for controlling the rotational speed and direction of the step-motor, therefore, the paths of the mobile sensor cars, was developed using Si Programmer (Applied Motion Products, 2009). Starting as shown in Figure 4a, the sensor cars traveled in unison at about 114 mm/s (4.5 in/s), while sampling acceleration at 280 Hz, toward the other support; as soon as the cars passed the East support, they reversed and returned to their initial positions. In each direction, the sensors scanned 7,788 points across the span. According to the mobile sensing protocol, the cars scanned the same 7,788 points on their return, resulting in 15,576 samples total (about 56 sec). Several bumps, with known locations, were installed on the surface of the beam to examine the precision of the spatiotemporal grid established by the step-motor and discrete-time sampling. The positions of the sensor cars provided by the motor program were estimated within 1.3% of the true positions.

During data collection, the plate was excited manually by two lab assistants, who applied impulse-like forces of moderate intensities at various locations along the main span to excite multiple modes. For validation of the estimated modal properties, acceleration data

was collected from the specimen using a network of four wireless fixed sensors (stationary sensor cars). The SID procedures and results for the mobile and fixed sensor networks are discussed in the following sections.

5.2 Practical considerations for DSN data processing and VPL selection

In practice, a continuous structure is scanned, as opposed to discretized elements in computer simulations. It is important to review details of DSN data and VPLs in this context. Although this article focuses on a specific subcategory of structures for validation, the formulation is based on general concepts, with applications exceeding this subcategory.

During measurement, the locations of the mobile sensors must be recorded or tracked by some means to establish the spatiotemporal grid, that is, sensing nodes and sensor-position time-series. In simulations, this task is trivial because it is a prerequisite for producing the DSN data. Furthermore, the units of the position entries are arbitrary, yet because they are a component of the DSN data set; it is recommended they are programmed with intuition to simplify the organization and interpretation of multiple analyses.

The experiment in this article exemplifies the case in which the locations of the sensors the positions are known with high certainty. In the case of smartphones, sensor-position vectors can be modeled by integrating associated sensor data, for example, GPS, accelerometer, gyroscope, and so on—a procedure with an estimation accuracy and precision that is independent of STRIDEX.

Generally, for sensors within moving vehicles, the measured signals are subject to noise generated through dynamic vehicle-bridge interaction (Cantieni, 1992; Jiang et al., 2004; Ward and Iagnemma, 2009; Yang and Chang, 2009), which is dependent on bridge dynamics, vehicle dynamics, vehicle speed, and road profile. In this application, the vibrations of the beam dominated the recorded signal because (i) the sensor cars are much stiffer than the beam specimen; (ii) the beam surface is smoothed with a layer of paper; and (iii) the sensor cars are not moving quickly. This study focuses on an experimental validation of the STRIDEX method; a comprehensive study on the impact of these parameters on identification is reserved for future work.

Finally, the VPLs need not coincide with any of the points scanned during measurement because the domain of the *sinc* interpolation function is continuous, that is, VPLs can be chosen in-between sensing nodes. As a result, the mode shape estimates that follow exist in a continuum; theoretically, their spatial resolutions are unlimited.

5.3 VPLs, SID results, and discussion

The network of two mobile sensors corresponded to an online DSN data matrix with two measurement channels, $N_{mc} = 2$, and two observations, $N_O = 2$. For minimum model size, each VPL set contained two points, that is, $N_\alpha = 2$ and $M = N_\alpha$. The VPLs are virtual points that are established in the TPM; although, with real structures, they also have an explicit representation in physical space. In each set, the VPLs were separated by 1.22 m (4 ft, 40% of the main span). The VPL sets were generated as uniformly shifted versions of one another. For instance, the points of one VPL set were spaced about 12.1 mm (0.48 in, 0.4% of the main span) from the adjacent set. Overall, 144 VPL sets were analyzed (144 STRIDEX runs, thus 144 sets of modal property estimates), which corresponded to 288 aggregate mode shape ordinates.

The fixed sensor data was collected by four stationary sensor cars and was processed independently using two SID methods: ERA-NExT (James et al., 1993) and STRIDE (Matarazzo and Pakzad, 2016c). The free, Matlab-based Structural Modal Identification Toolsuite (SMIT) (Chang and Pakzad, 2013b) program was selected to implement ERA-NExT 50 times at even models orders 2–100, and construct the corresponding stabilization diagram. Because the modal estimates can vary significantly among model orders (Chang and Pakzad, 2013b), the results from ERA-NExT model order 74 ($p = 74$) were selected to represent the method because they were consistent with the mean frequency and damping estimates of all model orders. The STRIDE method processed the data at a model order of four and with the default slope threshold ($p = 4$, $\theta = 5 \times 10^{-4}$). The initial state and observation matrices were provided by ERA-OKID-OO (Chang and Pakzad, 2013b) at model order four and the remainder of the superparameter was the default assignment.

The mobile sensor data was processed using STRIDEX at a model order of six and the default slope threshold ($p = 6, \theta = 5 \times 10^{-4}$). Recall with STRIDE, a higher model order can be selected to force further system poles using fewer sensors, for example, $N_{mc} = 2$. The same practice is applicable to STRIDEX in cases where the DSN data contain few observations, for example, $N_O = 2$. Initial estimates for the TPM state and observation matrices were provided by ERA-OKID-OO (Chang and Pakzad, 2013b) at model order six, with the remaining parameters set as the defaults.

The frequency and damping estimates for the first mode of the structure are provided in Table 3. The mean frequency and damping values for the 50 ERA-NExT estimates are shown as "ERA-NExT mean" and those

Table 3
A comparison of frequency and damping estimates for the first vertical mode: "ERA-NExT mean" are the average values out of 50 model orders considered; "ERA-NExT ($p = 74$)" are the estimates from model order 74; and "STRIDE" are the estimates from model order 4

SID method	*Frequency (Hz)*	*Damping (%)*
ERA-NExT mean	8.225	0.8914
ERA-NExT ($p = 74$)	8.237	0.8937
STRIDE	8.226	1.035
STRIDEX mean	8.304	0.7069
ERA-NExT CoV	2.059×10^{-3}	993.4×10^{-3}
STRIDEX CoV	2.077×10^{-3}	187.8×10^{-3}

from model order 74 are "ERA-NExT ($p = 74$)"; corresponding CoV values are also displayed. Similarly, the mean and CoV values of the 144 STRIDEX runs are indicated as "STRIDEX mean" and "STRIDEX CoV"; the mean values are interpreted as the modal estimates from the mobile sensor data. The frequency estimates of the fixed sensor data and the mobile sensing data are in agreement. The STRIDE and ERA-NExT estimates are slightly lower than those from STRIDEX, yet they are all within 1% of each other. Furthermore, the CoV of the STRIDEX estimates are on the same magnitude as those observed in the ERA-NExT stabilization diagram, demonstrating high precision.

The damping estimates are quite consistent among the different data sets and SID methods considered. The estimation of damping for a real structure through output-only SID is particularly challenging; not only are such estimates often accompanied with a larger standard deviation but the true values are unavailable for comparison (Au, 2013; Chang and Pakzad, 2013b; Matarazzo and Pakzad, 2015; Pakzad and Fenves, 2009). Given these challenges, the STRIDEX damping estimates are promising because they fit well with those computed using fixed sensor data. Finally, the CoV of the STRIDEX damping estimates have the same magnitude as those seen in the stabilization diagram of ERA-NExT. These results indicate that the accuracy and precision standards of fixed sensor networks and existing SID methods are also achievable with mobile sensing data and STRIDEX, which is quite encouraging.

The ordinates of the first mode shape are compared in Figure 5. With the DSN data and the scalable VPL strategy, 288 raw points were available. The spacing and the generation of the VPLs were such that 40 x-coordinates near midspan had two corresponding modal ordinates; only one modal ordinate is plotted for each point on the span. The resulting mode shape was scaled and shifted mildly in the x-direction to align its zero ordinates with

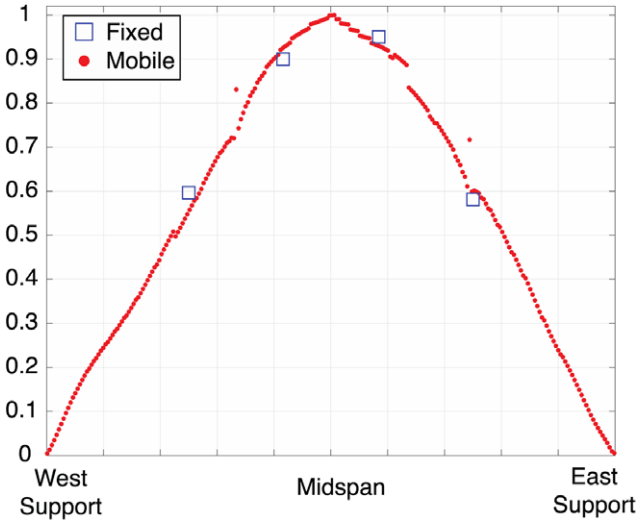

Fig. 5. First mode shape of the beam specimen: the mode shape estimated from the mobile sensor data contains 248 points.

Table 4
A comparison of the first mode shape using modal assurance criterion (MAC): the SID results from the fixed sensors (ERA-NExT and STRIDE) are compared with one another and then with those from the mobile sensors (STRIDEX)

SID methods	*MAC*
ERA-NExT ($p = 74$) & STRIDE	1.000
ERA-NExT ($p = 74$) & STRIDEX	0.9935
STRIDE & STRIDEX	0.9935

the supports. Finally, the mode shape was normalized to have a maximum value of one.

Figure 5 shows 248 ordinates computed from the mobile sensor data and four points produced from the fixed sensor data. In other words, each mobile sensor produced over 120 more mode shape points than each fixed sensor. This result further quantifies how DSN data sets can store dense spatial information efficiently in a compact data matrix. The "fixed" points shown in Figure 5 were computed using STRIDE and were identical to those estimated by ERA-NExT (as indicated by a MAC value of unity in Table 4). The accuracy of the high-resolution mode shape could only be verified at four points due to the limited size of the fixed sensor network. In Table 4, the mode shape estimates from three methods are compared with one another using the MAC (Allemang and Brown, 1982) metric, in which a value of one signifies perfect consistency between the mode shape vectors. The MAC between the STRIDEX mode shape and either fixed sensor estimate exceeded 0.99, indicating excellent consistency.

In summary, this experimental application further established how frequency and damping estimates obtained through SID with mobile sensor data and STRIDEX are on par with modern techniques that consider fixed sensor data. The dense mode shape estimate with 248 points exemplified the rich spatial information available in DSN data and successfully demonstrated its extraction through a series of STRIDEX runs.

6 SUMMARY AND CONCLUSIONS

- The rate at which the SHM community incorporates crowdsourced smartphone data depends on the adaptability and computational scalability of upcoming analytical tools. For instance, an output-only modal identification method that is capable of processing DSN data is also applicable to smartphone data.
- The STRIDEX algorithm was proposed for output-only modal identification of the stochastic TPM using DSN data, that is, mobile sensor data or BIGDATA.
- The STRIDEX identification algorithm has four key features:

    1. Comprehensive and convenient: estimates frequencies, damping, and mode shapes simultaneously.
    2. Adaptable: there are no methodological restrictions on sensor arrangement or mobility as long as the positions of each sensor are known for all samples.
    3. Scalable information: with a new VPL assignment, an additional identification run can produce a new set of mode shape ordinates from the same set of DSN data.
    4. Computationally scalable: (i) the size of the TPM is independent of the density of the spatial grid applied during measurement and (ii) in the construction of high-resolution mode shapes, the computational needs of individual runs are nearly equivalent to one another.

- With STRIDEX, the mode shape estimates of a real structure exist in a continuum; theoretically, their spatial resolutions are unlimited.
- It was shown that the accuracy and precision standards established by fixed sensor SID methods, for example, ERA-NExT and STRIDE, are also achievable using mobile sensors and STRIDEX.
- In a simulation where a network of six mobile sensors scanned a 5,000-DOF beam, the STRIDEX method demonstrated its ability to provide reliable modal property estimates of frequencies and damping ratios for the first four modes. A series of independent STRIDEX runs produced mode shape estimates with 24 points each (four times more points per sensor than a fixed sensor network) and were nearly perfectly consistent with the exact values.
- In an experimental application, two mobile sensor cars measured acceleration from about 8,000 points on a beam specimen in less than 1 minute. By compiling results from a series of independent STRIDEX runs, a dense mode shape with 248 ordinates (over 120 times more efficient than a fixed sensor network) was produced with a verified accuracy at four points, further proving the utility of an adaptable and scalable SID method.

ACKNOWLEDGMENTS

Research funding is partially provided by the National Science Foundation through Grant No. CMMI-1351537, by the Hazard Mitigation and Structural Engineering program, and by a grant from the Commonwealth of Pennsylvania, Department of Community and Economic Development, through the Pennsylvania Infrastructure Technology Alliance (PITA). We would like to thank Matthew Horner, Bhavana Valeti, Kate Kosner, and Soheil Sadeghi at Lehigh University for their assistance with experimentation setup and data collection.

REFERENCES

Abdel Wahab, M. M. & De Roeck, G. (1999), Damage detection in bridges using modal curvatures: application to a real damage scenario, *Journal of Sound and Vibration*, **226**(2), 217–35.

Adeli, H. (2001), Neural networks in civil engineering: 1989–2000, *Computer-Aided Civil and Infrastructure Engineering*, **16**(2), 126–42.

Adeli, H. & Jiang, X. (2006), Dynamic fuzzy wavelet neural network model for structural system identification, *Journal of Structural Engineering*, **132**(1), 102–11.

Alessandroni, G., Klopfenstein, L. C., Delpriori, S., Dromedari, M., Luchetti, G., Paolini, B. D., Seraghiti, A., Lattanzi, E., Freschi, V., Carini, A. & Bogliolo, A. (2014), SmartRoadSense: collaborative road surface condition monitoring, *Ubicomm* **2014**, 210–15.

Allemang, R. J. & Brown, D. L. (1982), A correlation coefficient for modal vector analysis, *Proceedings of the 1st International Modal Analysis Conference*, **1**, 110–16.

Applied Motion Products. (2009), Si Programmer™ software manual, http://www.applied-motion.com/sites/default/files/Si_Programmer_Software_Manual.pdf, accessed May 12, 2015.

Au, S.-K. (2013), Uncertainty law in ambient modal identification—part II: implication and field verification, *Mechanical Systems and Signal Processing*, **48**(1–2), 34–48.

Bamieh, B. & Giarré, L. (2002), Identification of linear parameter varying models, *International Journal of Robust and Nonlinear Control*, **12**(9), 841–53.

Box, G. E. P., Jenkins, G. M. & Reinsel, G. C. (2008), *Time Series Analysis: Forecasting and Control*, John Wiley & Sons, Inc., Hoboken, NJ.

Calabrese, F., Colonna, M., Lovisolo, P., Parata, D. & Ratti, C. (2011), Real-time urban monitoring using cell phones: a case study in Rome, *IEEE Transactions on Intelligent Transportation Systems*, **12**(1), 141–51.

Cantieni, R. (1992), *Dynamic Behavior of Highway Bridges Under the Passage of Heavy Vehicles*, EMPA Report No. 220, Dübendorf, Switzerland.

Carden, P. & Brownjohn, J. M. W. (2008), ARMA modelled time-series classification for structural health monitoring of civil infrastructure, *Mechanical Systems and Signal Processing*, **22**(2), 295–314.

Cha, Y. J., Trocha, P. & Büyüköztürk, O. (2016), Field measurement-based system identification and dynamic response prediction of a unique MIT building, *Sensors*, **16**(7), 1016.

Chandrashekhar, M. & Ganguli, R. (2009), Structural damage detection using modal curvature and fuzzy logic, *Structural Health Monitoring*, **8**(4), 267–82.

Chang, M. & Pakzad, S. N. (2013a), Modified natural excitation technique for stochastic modal identification, *Journal of Structural Engineering*, **139**(10), 1753–62.

Chang, M. & Pakzad, S. N. (2013b), Observer Kalman filter identification for output-only systems using interactive structural modal identification toolsuite (SMIT), *Journal of Bridge Engineering*, **19**(5), 04014002.

Chang, M. & Pakzad, S. N. (2014), Optimal sensor placement for modal identification of bridge systems considering number of sensing nodes, *Journal of Bridge Engineering*, **19**(6), 04014019.

Chang, M. & Pakzad, S. N. (2015), Optimal sensor configuration for flexible structures with multi-dimensional mode shapes, *Smart Materials and Structures*, **24**(5), 055012.

Eriksson, J., Girod, L., Hull, B., Newton, R., Madden, S. & Balakrishnan, H. (2008), The pothole patrol: using a mobile sensor network for road surface monitoring, *in Proceedings of the 6th International Conference on Mobile Systems, Applications, and Services*, ACM.

Feng, M., Fukuda, Y., Mizuta, M. & Ozer, E. (2015), Citizen sensors for SHM: use of accelerometer data from smartphones, *Sensors*, **15**(2), 2980–98.

Gao, Y., Spencer, B. F. & Ruiz-Sandoval, M. (2006), Distributed computing strategy for structural health monitoring, *Structural Control and Health Monitoring*, **13**(1), 488–507.

Gonzalez, A., O'Brien, E. J. & McGetrick, P. J. (2012), Identification of damping in a bridge using a moving instrumented vehicle, *Journal of Sound and Vibration*, **331**(18), 4115–31.

Guo, H. Y., Zhang, L. L., Zhang, L. L. & Zhou, J. X. (2004), Optimal placement of sensors for structural health monitoring using improved genetic algorithms, *Smart Materials and Structures*, **13**(3), 528–34.

Herrera, J. C., Work, D. B., Herring, R., Ban, X. (Jeff), Jacobson, Q. & Bayen, A. M. (2010), Evaluation of traffic data obtained via GPS-enabled mobile phones: the Mobile Century field experiment, *Transportation Research Part C: Emerging Technologies*, **18**(4), 568–83.

Horner, M., Kosner, K., Korneva, K., Matarazzo, T. J. & Pakzad, S. N. (2015), A wireless mobile sensor platform for structural health monitoring, *Proceedings of the Joint 6th International Conference on Advances in Experimental Structural Engineering (6AESE) and 11th International Workshop on Advanced Smart Materials and Smart Structures Technology (11ANCRiSST)*, Urbana-Champaign, IL, 1–7.

Hotel News Resource (2015), Internet of things (iot): number of connected devices worldwide from 2012 to 2020 (in billions), *Statista—The Statistics Portal*. Statista, https://www.statista.com/statistics/471264/iot-number-of-connected-devices-worldwide/, accessed October 21, 2016.

Huang, Y., Beck, J. L., Wu, S. & Li, H. (2014), Robust Bayesian compressive sensing for signals in structural health monitoring, *Computer-Aided Civil and Infrastructure Engineering*, **29**(3), 160–79.

James III, G. H., Carne, T. G. & Lauffer, J. P. (1993), *The Natural Excitation Technique (NExT) for Modal Parameter Extraction from Operating Wind Turbines*, No. SAND-92-1666, Sandia National Labs., Albuquerque, NM.

Jang, S., Jo, H., Cho, S., Mechitov, K., Rice, J. A., Sim, S. H., Jung, H. J., Yun, C. B., Spencer, B. F. & Agha, G. (2010), Structural health monitoring of a cable-stayed bridge using smart sensor technology: deployment and evaluation, *Smart Structures and Systems*, **6**(5), 439–59.

Jiang, R. J., Au, F. T. K. & Cheung, Y. K. (2004), Identification of vehicles moving on continuous bridges with rough surface, *Journal of Sound and Vibration*, **274**(3–5), 1045–63.

Kijewski-Correa, T., Kwon, D. K., Kareem, A., Bentz, A., Guo, Y., Bobby, S. & Abdelrazaq, A. (2013), SmartSync: an integrated real-time structural health monitoring and structural identification system for tall buildings, *Journal of Structural Engineering*, **139**(10), 1675–87.

Kim, S., Yoon, C. & Kim, B. (2000), Structural monitoring system based on sensitivity analysis and a neural network, *Computer-Aided Civil and Infrastructure Engineering*, **15**(15), 309–18.

Ko, J. M. & Ni, Y. Q. (2005), Technology developments in structural health monitoring of large-scale bridges, *Engineering Structures*, **27**(12 SPEC. ISS.), 1715–25.

Kotelnikov, V. A. (1933), On the transmission capacity of the 'ether' and of cables in electrical communications, in *Proceedings of the First All-Union Conference on the Technological Reconstruction of the Communications Sector and the Development of Low-Current Engineering*, Moscow, 1–23.

Kumar, R., Mukherjee, A. & Singh, V. P. (2016), Community sensor network for monitoring road roughness using smartphones, *Journal of Computing in Civil Engineering*, **4016059**, 1–11.

Kurata, M., Kim, J., Lynch, J. P., Van der Linden, G., Sedarat, H., Thometz, E., Hipley, P. & Sheng, L. (2013), Internet-enabled wireless structural monitoring systems: development and permanent deployment at the New Carquinez Suspension Bridge, *Journal of Structural Engineering*, **139**(10), 1688–702.

Kurata, M., Kim, J., Zhang, Y., Lynch, J. P., Van Der Linden, G. W., Jacob, V., Thometz, E., Hipley, P. & Sheng, L. -H. (2011), Long-term assessment of an autonomous wireless structural health monitoring system at the New Carquinez Suspension Bridge, *Nondestructive Characterization for Composite Materials, Aerospace Engineering, Civil Infrastructure, and Homeland Security*, **7983**(2011), 798312.

Laney, D. (2001), 3D data management: controlling data volume, velocity and variety, *META Group Research Note* **6**(2001), 70.

Lee, L. & Poolla, K. (1999), Identification of linear parameter-varying systems using nonlinear programming, *Journal of Dynamic System Measurement and Control*, **121**(1), 71–78.

Lin, C. W. & Yang, Y. B. (2005), Use of a passing vehicle to scan the fundamental bridge frequencies: an experimental verification, *Engineering Structures*, **27**(13), 1865–78.

Lynch, J. P. (2002), *Decentralization of wireless monitoring and control technologies for smart civil structures*. Ph.D. thesis, Stanford University. Available at: http://eil.stanford.edu/publications/jerry_lynch/jerry_thesis.pdf, accessed August 2017.

Lynch, J. P. (2007), An overview of wireless structural health monitoring for civil structures, *Philosophical Transactions. Series A, Mathematical, Physical, and Engineering Sciences*, **365**(1851), 345–72.

Lynch, J. P., Wang, Y., Loh, K. J., Yi, J.-H. & Yun, C.-B. (2006), Performance monitoring of the Geumdang Bridge using a dense network of high-resolution wireless sensors, *Smart Materials and Structures*, **15**(6), 1561–75.

Marulanda, J., Caicedo, J. M. & Thomson, P. (2016), Modal identification using mobile sensors under ambient excitation, *Journal of Computing in Civil Engineering*, **31**(2), 04016051.

Matarazzo, T. J., Horner, M., Kosner, K. & Pakzad, S. N. (2016a), Multiphase mobile sensor network for beam health monitoring, in T. N. Bittencourt, D. M. Frangopol & A. Beck (eds.), *Maintenance, Monitoring, Safety, Risk and Resilience of Bridges and Bridge Networks*, Taylor & Francis Group, London, 186.

Matarazzo, T. J., Horner, M. & Pakzad, S. N. (2016b), High-resolution mode shape identification using mobile sensors, in *Topics in Modal Analysis & Testing*, vol. 10, Springer, Cham, 255–60.

Matarazzo, T. J. & Pakzad, S. N. (2015), Sensitivity metrics for maximum likelihood system identification, *ASCE-ASME Journal of Risk and Uncertainty in Engineering Systems, Part A: Civil Engineering*, **2**(3), B4015002.

Matarazzo, T. J. & Pakzad, S. N. (2016a), Structural modal identification for mobile sensing with missing observations, *Journal of Engineering Mechanics*, **142**(5), 04016021.

Matarazzo, T. J. & Pakzad, S. N. (2016b), Truncated physical model for dynamic sensor networks with applications in high-resolution mobile sensing and BIGDATA, *Journal of Engineering Mechanics*, **142**(5), 04016019.

Matarazzo, T. J. & Pakzad, S. N. (2016c), STRIDE for structural identification using expectation maximization: iterative output-only method for modal identification, *Journal of Engineering Mechanics*, **142**(4), 04015109.

Matarazzo, T. J., Shahidi, S. G., Chang, M. & Pakzad, S. N. (2015a), Are today's SHM procedures suitable for tomorrow's BIGDATA?, in *Proceedings of the Society of Experimental Mechanics IMAC XXXIII, Orlando, FL. Structural Health Monitoring and Damage Detection*, vol. 7, Springer, Cham, 59–65.

Matarazzo, T. J., Shahidi, S. G. & Pakzad, S. N. (2015b), Exploring the efficiency of BIGDATA analyses in SHM, in F.-K. Chang (ed.). *Proceedings of the 10th International Workshop on Structural Health Monitoring*, Stanford, CA, 2981–89.

MediaPost (2015), Number of smartphone users in the United States from 2010 to 2019 (in millions)*, *Statista*, https://www.statista.com/statistics/201182/forecast-of-smartphone-users-in-the-us/, accessed October 4, 2016.

Meo, M. & Zumpano, G. (2005), On the optimal sensor placement techniques for a bridge structure.pdf, *Engineering Structures*, **27**, 1488–97.

Mohan, P., Padmanabhan, V. N. & Ramjee, R. (2008), Nericell: rich monitoring of road and traffic conditions using mobile smartphones, in *Proceedings of the 6th ACM Conference on Embedded Network Sensor Systems—SenSys '08*, ACM, Raleigh, NC, 323–36.

Moheimani, S. O. R., Halim, D. & Fleming, A. J. (2003), System identification for spatially distributed systems, in A. Guran, C. Christov, M. Cloud, F. Pichler, and W. B. Zimmerman (eds.), *Spatial Control of Vibration: Theory and Experiments*, World Scientific, Singapore.

Ni, Y., Xia, Y., Liao, W. Y. & Ko, J. M. (2009), Technology innovation in developing the structural health monitoring system for Guangzhou New TV Tower, *Structural Control and Health Monitoring*, **16**, 73–98.

Nigro, M. B., Pakzad, S. N. & Dorvash, S. (2014), Localized structural damage detection: a change point analysis, *Computer-Aided Civil and Infrastructure Engineering*, **29**(6), 416–32.

O'Connor, S. M., Lynch, J. P. & Gilbert, A. C. (2014), Compressed sensing embedded in an operational wireless sensor network to achieve energy efficiency in long-term monitoring applications, *Smart Materials and Structures*, **23**(8), 085014.

Pakzad, S. N. & Fenves, G. L. (2009), Statistical analysis of vibration modes of a suspension bridge using spatially dense wireless sensor network, *Journal of Structural Engineering*, **135**(7), 863–72.

Pakzad, S. N., Fenves, G. L., Kim, S. & Culler, D. E. (2008), Design and implementation of scalable wireless sensor network for structural monitoring, *Journal of Infastructure Systems*, **14**(1), 89–101.

Pandey, A. K., Biswas, M. & Samman, M. M. (1991), Damage detection from changes in curvature mode shapes, *Journal of Sound and Vibration*, **145**(2), 321–32.

Pew Research Center (2016), *Smartphone Ownership and Internet Usage Continues to Climb in Emerging Economies*. Pew Research Center. Available at: http://s1.pulso.cl/wp-content/uploads/2016/02/2258581.pdf, accessed August 2017.

Qarib, H. & Adeli, H. (2015), A new adaptive algorithm for automated feature extraction in exponentially damped signals for health monitoring of smart structures, *Smart Materials and Structures*, **24**(12), 125040.

Shahidi, S. G., Nigro, M. B., Pakzad, S. N. & Pan, Y. (2015), Structural damage detection and localisation using multivariate regression models and two-sample control statistics, *Structure and Infrastructure Engineering*, **11**(10), 277–93.

Shannon, C. E. (1998), Communication in the presence of noise, *Proceedings of the IEEE*, **86**(2), 447–57.

Siringoringo, D. M. & Fujino, Y. (2012), Estimating bridge fundamental frequency from vibration response of instrumented passing vehicle: analytical and experimental study, *Advances in Structural Engineering*, **15**(3), 417–34.

Smarsly, K., Law, K. H. & Hartmann, D. (2012), Multiagent-based collaborative framework for a self-managing structural health monitoring system, *Journal of Computing in Civil Engineering*, **26**(1), 76–89.

Soyoz, S. & Feng, M. Q. (2009), Long-term monitoring and identification of bridge structural parameters, *Computer-Aided Civil and Infrastructure Engineering*, **24**(2), 82–92.

Spencer, Jr., B. F. (2011), Getting Started Guide for New Users—Programming the ISHMP Toolsuite V3.0 and Collecting Data with Imote2s.

Spencer, B. F., Ruiz-Sandoval, M. E. & Kurata, N. (2004), Smart sensing technology: opportunities and challenges, *Structural Control and Health Monitoring*, **11**(4), 349–68.

Spiridonakos, M. D., Chatzi, E. N. & Sudret, B. (2016), Polynomial chaos expansion models for the monitoring of structures under operational variability, *ASCE-ASME Journal of Risk and Uncertainty in Engineering Systems, Part A: Civil Engineering*, **2**(3), B4016003.

Sun, H. & Betti, R. (2015), A hybrid optimization algorithm with Bayesian inference for probabilistic model updating, *Computer-Aided Civil and Infrastructure Engineering*, **30**(8), 602–19.

Toth, R. (2010), *Modeling and Identification of Linear Parameter-Varying Systems*, Springer-Verlag Berlin Heidelberg.

Tóth, R., Heuberger, P. S. C. & Van den Hof, P. M. J. (2009), Asymptotically optimal orthonormal basis functions for LPV system identification, *Automatica*, **45**(6), 1359–70.

Unnikrishnan, J. & Vetterli, M. (2012), *Sampling and Reconstructing Spatial Fields Using Mobile Sensors. 2012 IEEE International Conference on Acoustics, Speech and Signal Processing (ICASSP)*, IEEE, Berkeley, CA.

Verdult, V. & Verhaegen, M. (2002), Subspace identification of multivariable linear parameter-varying systems, *Automatica*, **38**(5), 805–14.

Ward, C. C. & Iagnemma, K. (2009), Speed-independent vibration-based terrain classification for passenger vehicles, *Vehicle System Dynamics*, **47**(9), 1095–113.

Whittaker, E. T. (1915), On the functions which are represented by the expansions of interpolation-theory, *Proceedings of the Royal Society of Edinburgh*, **35**(1915), 181–94.

Whittaker, J. M. (1929), The 'Fourier' theory of the cardinal function, in *Proceedings of the Edinburgh Mathematical Society*, **1**(December 1927), 169–76.

Yang, Y. B. & Chang, K. C. (2009), Extracting the bridge frequencies indirectly from a passing vehicle: parametric study, *Engineering Structures*, **31**(10), 2448–59.

Yang, Y.-B., Lin, C. W. & Yau, J. D. (2004), Extracting bridge frequencies from the dynamic response of a passing vehicle, *Journal of Sound and Vibration*, **272**(3–5), 471–93.

Yao, R. & Pakzad, S. N. (2012), Autoregressive statistical pattern recognition algorithms for damage detection in civil structures, *Mechanical Systems and Signal Processing*, **31**, 355–68.

Yao, R., Pakzad, S. N. & Venkitasubramaniam, P. (2017), Compressive sensing based structural damage detection and localization using theoretical and metaheuristic statistics, *Structural Control and Health Monitoring*, **24**(4), https://doi.org/10.1002/stc.1881.

Yuen, K. V. & Mu, H. Q. (2015), Real-time system identification: an algorithm for simultaneous model class selection and parametric identification, *Computer-Aided Civil and Infrastructure Engineering*, **30**(10), 785–801.

Zhang, Y., O'Connor, S. M., van der Linden, G. W., Prakash, A. & Lynch, J. P. (2016), SenStore: a scalable cyberinfrastructure platform for implementation of data-to-decision frameworks for infrastructure health management, *Journal of Computing in Civil Engineering*, **30**(5), 04016012.

Zhu, D., Guo, J., Cho, C., Wang, Y. & Lee, K. (2012), Wireless mobile sensor network for the system identification of a space frame bridge, *IEEE/ASME Transactions on Mechatronics*, **17**(3), 499–507.

Zhu, D., Yi, X., Wang, Y., Lee, K.-M. & Guo, J. (2010), A mobile sensing system for structural health monitoring: design and validation, *Smart Materials and Structures*, **19**(5), 1–11.

NOTATION

The following symbols were used in this article:

Symbol	*Description*
A	TPM state matrix; size is $pN_\alpha \times pN_\alpha$. For minimum model size: $N_\alpha = N_O = M$
C	TPM observation matrix; size is $M \times pN_\alpha$.
$C_k^{(eq)}$	Equivalent time-variant observation matrix exclusively defined for E-step; equal to $\Omega_k C$; size is $N_O \times pN_\alpha$
p	Model order; scalar
$\boldsymbol{s}^\alpha$	Location vector of N_α VPLs in TPM; size is N_α; element is s_i^α
$\boldsymbol{s}_k^O$	Location vector of N_O observations at time-step k; size is N_O
Δs^α	Distance between uniformly spaced VPLs
j	Iteration index; integer
θ	Log-likelihood slope threshold; scalar
k	Time-step index; integer
K	Total number of time steps; integer
$\boldsymbol{x}_k$	State vector in TPM; size is pN_α. For minimum model size: $N_\alpha = N_O = M$
$\tilde{\boldsymbol{\mu}}$	Mean vector for initial state vector $\boldsymbol{x}_1$; size is pN_α
$\tilde{V}$	Covariance matrix for initial state vector $\boldsymbol{x}_1$; size is $pN_\alpha \times pN_\alpha$
$\boldsymbol{y}_k$	Observation vector in TPM; size is N_O
Y	Aggregated observations (DSN data)
N_α	Number of VPLs; integer
N_O	Number of observations; integer
N_{mc}	Number of measurement channels; integer
N	Number of sensing nodes; integer
M	Number of modes in TPM; integer
Ψ_j	Superparameter for TPM at iteration j
Ω_k	Mode shape regression (MSR) term; size is $N_O \times M$.
$\hat{\Omega}_k$	Approximation of MSR term using *sinc* basis
$\boldsymbol{\eta}_k$	Gaussian state input vector; size is pN_α
$\boldsymbol{v}_k$	Gaussian measurement noise vector; size is N_O
Q	State input covariance matrix; size is $pN_\alpha \times pN_\alpha$
R	Measurement noise covariance matrix; size is $N_O \times N_O$
$\hat{\boldsymbol{x}}_{k\|K}$	Minimum mean squared-error estimate of state vector at time-step k; size is pN_α
$\hat{V}_{k_1,k_2\|K}$	Covariance matrix for estimated states at time-steps k_1 and k_2; size is $pN_\alpha \times pN_\alpha$
$L_{X,Y}(\Psi_j)$	Complete data log-likelihood function for TPM; scalar
$G(\Psi_{j+1}\|\Psi_j)$	Conditional expectation of TPM log-likelihood function given observations and superparameter estimate at iteration j
Φ_k^O	Mode shape matrix containing ordinates at observation locations; size is $N_O \times M$
Φ^α	Mode shape matrix containing ordinates at VPLs; size is $N_\alpha \times M$
Λ	Diagonal eigenvalue matrix of A; size is $pN_\alpha \times pN_\alpha$
Γ	Eigenvector matrix A; size is $pN_\alpha \times pN_\alpha$
$\hat{\boldsymbol{f}}$	Vector of estimated modal frequencies; size is pN_α
$\hat{\zeta}$	Vector of estimated damping ratios; size is pN_α
$\hat{\Phi}$	Matrix of estimated mode shapes (at VPLs); size is $N_O \times pN_\alpha$
Δt	Sampling period in seconds; scalar